PCCP

PAPER

View Article Online
View Journal | View Issue

Cite this: *Phys. Chem. Chem. Phys.*, 2017, **19**, 29187

Design of an efficient coherent multi-site single-molecule rectifier†

Mickael L. Perrin,[ab] Matthijs Doelman,[a] Rienk Eelkema[c] and Herre S. J. van der Zant*[a]

Received 3rd July 2017,
Accepted 16th October 2017

DOI: 10.1039/c7cp04456a

rsc.li/pccp

We propose the design of a single-molecule diode with a rectification ratio exceeding a million. The employed mechanism is based on coherent resonant charge transport across a molecule that consists of four conjugated sites coupled by non-conjugated bridges. Using density functional theory calculations, we rationalize the design of the molecule and demonstrate the crucial role of aligning the sites at a specific voltage. Rectification ratios are calculated for a series of chemical substituents and demonstrate that with careful molecular design, high rectification ratios can be achieved. Finally, we comment on the shortcomings of our approach, how further improvements can be obtained and discuss some of the experimental challenges.

Molecular diodes have been attracting much attention recently, both in self-assembled monolayers[1–7] and on the single-molecule scale.[8–16] Even though the rectifier has been the seminal device which launched the field of single-molecule electronics,[17] up to date, their performance have many shortcomings. In particular, their rectification ratios (RR) are orders of magnitude lower than typical semiconducting rectifiers. The highest RR reported experimentally on a single-molecule junction[15] is about 600, and is no match for a semiconducting diode where ratios exceeding 10^6 are common. In that study, a molecular backbone was considered which consisted of two identical, weakly-coupled conjugated parts. In such a system, current flows coherently when both halves are on resonance, *i.e.*, the sites are aligned with each other within the bias window. The alignment of the two sites can be modified by applying a bias voltage and/or by chemical substituents. With proper design, one can align the sites at zero bias, while misaligning them at finite bias, yielding negative differential conductance.[18] One can also align the sites at a finite bias,[15,19–22] and achieve single-molecule rectification.

Based on a similar principle, here we investigate theoretically how the rectification ratio of single-molecule diodes can be significantly enhanced by the addition of more sites in series, as shown in as presented in Fig. 1b. Low RR are primarily caused by a high reverse current. Adding more sites in series leads to a strong suppression of the reverse current, thereby drastically improving the RR. However, the addition of sites comes at the cost of an increased molecular complexity and number of model parameters. In this study, we first focus on the design of a molecule which behaves as having four sites in series. For this purpose, we use density functional theory (DFT) calculations. We then investigate how the molecule can be engineered by the means of chemical substitution to align the sites at a particular bias voltage. We eventually show that the molecule designed with four sites represents a drastic improvement compared to a two-site molecule, with RR approaching 10^6, competitive with silicon-based diodes.

1 Design guidelines

Fig. 1 depicts the concept of a rectifier based on the four-site model. In Fig. 1a, the four sites are at energy ε_i, with $i = 1, 2, 3$ or 4, and weakly coupled to each other in series by τ_i ($i = 1, 2, 3$). At zero bias, the four sites are positioned like a staircase ($\varepsilon_1 > \varepsilon_2 > \varepsilon_3 > \varepsilon_4$). As the sites are not aligned, *i.e.*, they all possess a different energy, the transmission through such a configuration is low, as well as the conductance. Upon application of a bias voltage (see inset Fig. 1b), part of the voltage drops inside the molecule, leading to a shift of the on-site energies by $\alpha_i eV$ ($i = 1, 2, 3, 4$). The rest of the voltage drop is assumed to occur at the molecule/electrode interfaces. This voltage drop is crucial, as it allows for shifting the energies of

[a] *Kavli Institute of Nanoscience, Delft University of Technology, Lorentzweg 1, 2628 CJ Delft, The Netherlands. E-mail: H.S.J.vanderZant@tudelft.nl*
[b] *Swiss Federal Laboratories for Materials Science and Technology, Überlandstrasse 129, 8600 Dübendorf, Switzerland*
[c] *Department of Chemical Engineering, Delft University of Technology, Van der Maasweg 9, 2629 HZ, Delft, The Netherlands*

† Electronic supplementary information (ESI) available: DFT+NEGF calculations on the H–CCH–Cl–CN substituted C4-tetraene molecule for various values of $\Gamma_{L,R}$, construction of LMOs and MOs and calculations on the C4-tetraene with 2 sites only. The Supporting Information also provides the *xyz*-coordinates of the H–CCH–Cl–CN molecule, including the orbitals structure. See DOI: 10.1039/c7cp04456a

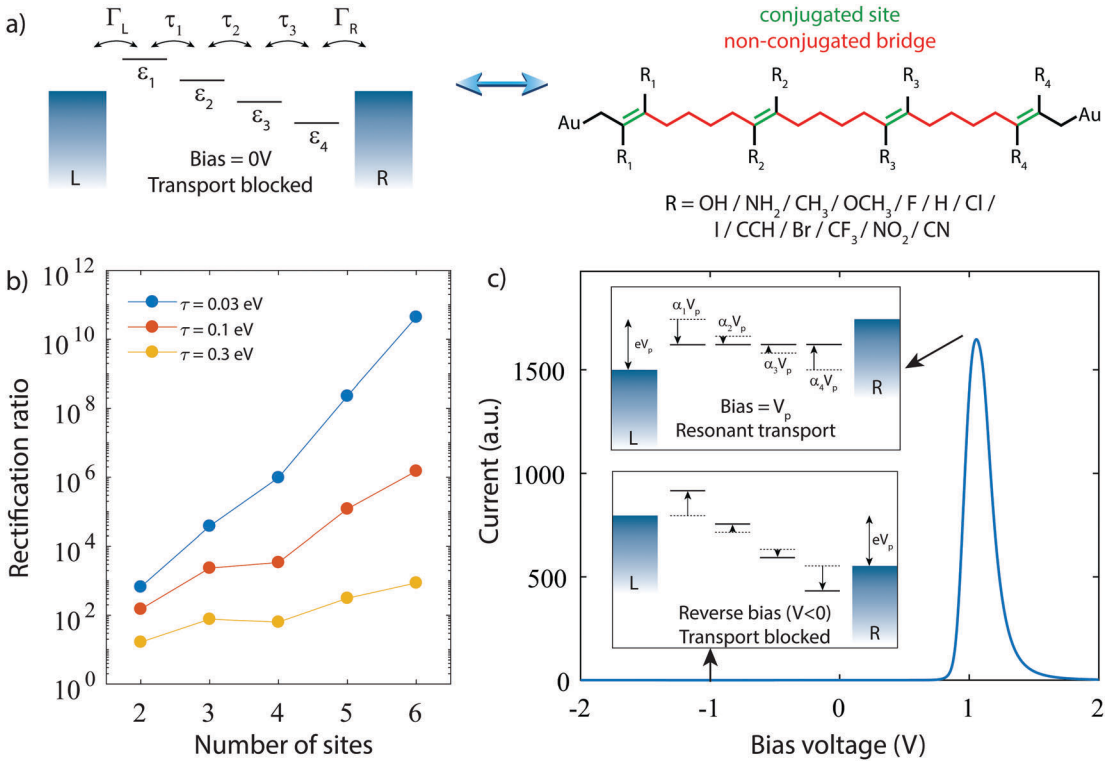

Fig. 1 Diode mechanism based on a four-site model. (a) Schematic representation of the four-site model with the sites positioned in a staircase (left) and the chemical structure of the C4-tetraene molecule, with the conjugated and non-conjugated parts highlighted (right). (b) Rectification ratio for an increasing number of sites for the following parameters: the on-site energies ε are linearly spaced between $\varepsilon_1 = 0.50$ eV and $\varepsilon_n = -0.5$ eV, the values of α are linearly spaced between $\alpha_1 = 0.50$ and $\alpha_n = -0.50$, and $\Gamma_{L,R} = 0.1$ eV. (c) Current–voltage characteristic (IV) calculated using the following parameters: $\varepsilon_1 = 0.50$ eV, $\varepsilon_2 = 0.167$ eV, $\varepsilon_3 = -0.167$ eV, $\varepsilon_4 = -0.50$ eV, $\alpha_1 = 0.50$, $\alpha_2 = 0.167$, $\alpha_3 = -0.167$, $\alpha_4 = -0.50$, $\tau_{1,2,3} = 0.03$ eV and $\Gamma_{L,R} = 0.1$ eV. The *IV* is highly asymmetric and shows a peak at 1 V. The insets show the site positioning for 1 V and −1 V. At the 1 V the sites are aligned and the current is high. At −1 V, the sites are misaligned and transport is blocked.

the sites, a key ingredient for aligning all of them at a particular finite bias voltage. At the voltage where the sites meet, both the conductance and the current are high. In the following, this bias voltage will be referred to as the operating voltage, and the bias polarity as forward bias. When increasing the bias even further, the sites start to misalign again and the current drops. For the opposite polarity (reverse bias), the sites never align and are increasingly shifted away from one other. The conductance therefore remains low, and the molecule behaves as a rectifier.

The Hamiltonian of the four-site model is given by

$$\boldsymbol{H} = \begin{pmatrix} \varepsilon_1 - \alpha_1 eV & -\tau_1 & 0 & 0 \\ -\tau_1 & \varepsilon_2 - \alpha_2 eV & -\tau_2 & 0 \\ 0 & -\tau_2 & \varepsilon_3 + \alpha_3 eV & -\tau_3 \\ 0 & 0 & -\tau_3 & \varepsilon_4 + \alpha_4 eV \end{pmatrix}, \quad (1)$$

with V the applied bias voltage and e the electron charge. Within the non-equilibrium Green function framework (NEGF), the energy-dependent transmission is given by[23–25]

$$\mathscr{T}(\varepsilon) = \mathrm{Tr}\{\boldsymbol{\Gamma}_L \boldsymbol{G}^r(\varepsilon) \boldsymbol{\Gamma}_R \boldsymbol{G}^a(\varepsilon)\}, \quad (2)$$

where $\boldsymbol{G}^r(\varepsilon)$ and $\boldsymbol{G}^a(\varepsilon)$ are the retarded and advanced Green's functions, respectively. The former is given by

$$\boldsymbol{G}^r(\varepsilon) = \left(\varepsilon \mathbf{1} - \boldsymbol{H} + \frac{i}{2}(\boldsymbol{\Sigma}_L + \boldsymbol{\Sigma}_R)\right)^{-1}, \quad (3)$$

with $\boldsymbol{G}^a(\varepsilon) = \boldsymbol{G}^r(\varepsilon)^\dagger$. $\boldsymbol{\Sigma}_{L,R}$ are the self-energy matrices and describe the coupling to the electrodes. Assuming wide-band limit electrodes and a symmetric coupling (see Section I of the ESI† for asymmetric coupling), $\boldsymbol{\Sigma}_{L,R}$ can be simplified to[24,25]

$$\boldsymbol{\Sigma}_L = \begin{pmatrix} \Gamma & 0 & 0 & 0 \\ 0 & 0 & 0 & 0 \\ 0 & 0 & 0 & 0 \\ 0 & 0 & 0 & 0 \end{pmatrix}, \quad \boldsymbol{\Sigma}_R = \begin{pmatrix} 0 & 0 & 0 & 0 \\ 0 & 0 & 0 & 0 \\ 0 & 0 & 0 & 0 \\ 0 & 0 & 0 & \Gamma \end{pmatrix}. \quad (4)$$

The current can be then calculated *via*[23–25]

$$I = \frac{2e}{\hbar}\int \frac{d\varepsilon}{2\pi}(f_L(\varepsilon) - f_R(\varepsilon))\mathscr{T}(\varepsilon), \quad (5)$$

where $f_L(\varepsilon)$ and $f_R(\varepsilon)$ are the Fermi–Dirac distributions of the left and right electrode, respectively. Fig. 1b shows the current as calculated from the four-site model Hamiltonian (eqn (1)) using eqn (5) for the current. The current–voltage (*IV*) characteristic

indeed shows a strong asymmetry. The current is low for all biases, at the exception of a peak at 1 V. At this operating voltage, the four energies are the same, and the maximum current and RR is achieved. We note that the operating voltage depends on the model parameters ε_i and α_i, and that with a careful choice of these parameters, *i.e.*, a careful design of the molecule, a large range of operating voltages, RR and peak currents can be obtained.

A single-molecule diode, in order to behave as four sites in series, needs to fulfill a few requirements. First of all, the molecule has to effectively behave as four-sites, meaning it should possess four conjugated parts, which are weakly coupled to each other. This also implies that the molecular orbitals behaving according to the four-site model should not interact, or at least very little, with other molecular orbitals. These additional orbitals may, for instance, lead to a parasitic current in the reverse bias mode, thereby deteriorating the RR. As the density of orbitals heavily depends on the total number of electrons in the system, key for minimizing undesirable orbital contributions is to reduce the number of electrons in the system. For this purpose, each site in the molecule shown in Fig. 1b consist of just a single ethylene unit, one of the smallest possible conjugated units. Second, the weak inter-site coupling is important, as it results in a voltage drop inside the molecule, and hence a Stark-shift of the orbitals. A weak inter-site coupling also enhances the RR as can be seen in Fig. 1b, and for this reason, butylene will be used. Third, the molecular orbitals described by the four-site model are required to be located closely to the Fermi energy of the electrodes, of which the alignment is strongly influenced by the anchoring groups. Here, we use gold electrodes, with a direct carbon–gold bond (Csp^3–Au) as anchoring. This anchoring promotes transport *via* the highest occupied molecular orbital[26–28] (HOMO). An important advantage of this anchoring group is also that it is chemically stable when directly bonded to the ethylene sites. This is not the case for typical anchoring groups such as thiols, or amines. Such groups, when directly bonded to an ethylene group, are prone to isomerize to the generally more stable thioketones or imines, thereby destroying both the ethylene site and the anchoring group. Furthermore, in the calculations we assume that at zero bias ($V = 0$) the HOMO is on resonance with the Fermi energy. Experimentally, this may require the presence of an electrochemical[29–31] or electrostatic[32] gate. However, we would like to stress that this assumption represents the ideal case with the highest rectification. As we will show further on in this study, the rectification ratio strongly depends on the level alignment; when the HOMO is several hundred meV off from the Fermi energy, rectification can decrease by several orders of magnitude.

The right panel of Fig. 1a presents the proposed molecule (with an icosa-1,7,13,19-tetraene backbone), which fulfills the above mentioned requirements. In the following, this molecule will be referred to as C4-tetraene. To control the energies of the sites, the electronegative/electronpositive chemical substituents (R_i) shown below the molecule will be employed.

2 Theoretical methods

Electronic structures were investigated using density functional theory (DFT) calculations, performed using the Amsterdam density functional (ADF) package with the GGA PBE exchange–correlation functional and the triple-ζ plus polarization (TZP) basis-set.[33,34] All geometries were converged to energy changes of less than 10^{-3} Hartree, energy gradients of less than 10^{-3} Hartree per Å maximum and 6.7×10^{-4} Hartree per Å RMS. Transmissions were then calculated from DFT within the non-equilibrium Green's function (NEGF) framework by coupling the molecule to wide-band electrodes[18,35] (with a coupling strength $\Gamma_{L,R}$ = 100 meV) involving the 6s atomic orbitals of the gold. Application of a bias voltage was performed by introducing a uniform electric field along the axis connecting the two gold atoms.

3 Results

As a starting point, we calculate the energy of the HOMO till HOMO−3 for the unsubstituted molecule (R_i = H) as a function of bias voltage (shown in Fig. 2a). At zero bias, the HOMO and HOMO−1 are nearly degenerate, with the HOMO−2 and HOMO−3 located about 0.5 and 0.6 eV lower in energy, respectively. For increasing bias voltage (both positive and negative), the orbitals are shifted in a pairwise manner, *i.e.*, the HOMO away from the HOMO−1, and the HOMO−2 away from the HOMO−3.

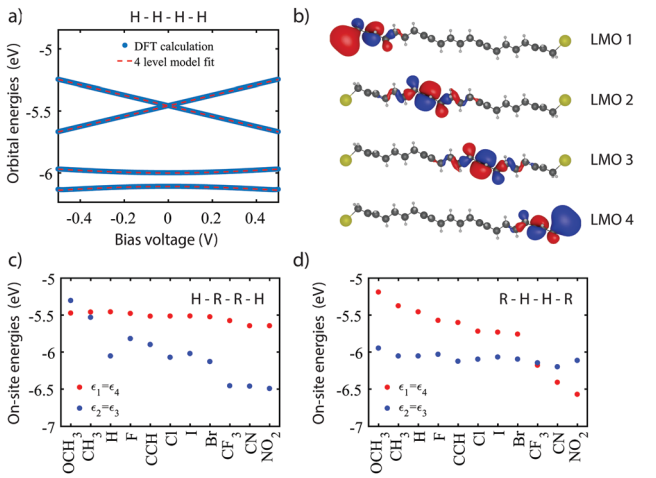

Fig. 2 DFT calculations on symmetrically substituted C4-tetraene molecules. (a) Bias dependent DFT calculation (blue) on the unsubstitutes molecule (H–H–H–H), fitted to the four-site model. The obtained fit parameters are $\varepsilon_{1,4}$ = −5.46 eV, $\varepsilon_{2,3}$ = −6.05 eV, $\alpha_{1,4}$ = 0.42, $\alpha_{2,3}$ = 0.13, $\tau_{1,3}$ = 5.2 meV, τ_2 = 54.6 meV. (b) Localized molecular orbitals for the H–H–H–H molecules, obtained from the molecular orbitals and the fit parameters obtained in (a). (c and d) One-site energies upon variation of the inner site (H–R–R–H) and outer site (R–H–H–R), respectively. In both cases, the energies of the unsubstituted sites remain fairly constant, while the substituted ones shift significantly. The chemical substituents have been sorted according to the energy shifts they induce in the two-site counterpart of the C4-tetraene molecule (see Section IV of the ESI†).

To obtain the model parameters, the DFT values are numerically fitted to the eigenvalues of the four-site Hamiltonian (eqn (1)). For symmetry reasons, the energies and shifts of the outer sites are equal. The same holds for the energies of the inner sites and the inter-site coupling. This reduces the number of parameters from 11 to 6. Fitting was performed as follows. First, by combining a constraint mean-square error minimization routine and an unconstrained nonlinear optimization routine, the on-site energies and inter-site couplings were determined. These were then fixed, and using a second unconstrained nonlinear optimization routine, the values of $\alpha_{1,2}$ were determined (for more details concerning the fitting procedure, see Section II of the ESI†). The model parameters were then used to calculate the four-site orbital energies, which are plotted on top of the DFT values. As can be seen in Fig. 2a, the four-site model describes the DFT calculations well, both the energy separation between the orbitals, as well as their shift with bias.

The DFT calculations also provide the orbital shape of the HOMO orbitals. Using the fitted model parameters, one can perform a basis transformation from the molecular orbitals (MOs) to the localized molecular orbitals (LMOs), *i.e.*, from the molecular orbitals one can obtain the electron density of the four basis functions (sites). For a more detailed description of the procedure, we refer to Section III of the ESI.† The LMOs are presented in Fig. 2b. Each LMO is localized on one of the sites, supporting the fact that charge transport in this molecule behaves according to the four-site model.

We will now investigate how the sites can be shifted by means of chemical substitution. As has been demonstrated previously,[20] chemical substitution can be used to influence the on-site energies. For this purpose, 11 substituents were chosen (see Fig. 1a), some of which are electronegative, whereas others are electropositive. First, the inner sites were varied symmetrically, while keeping the outer sites fixed (R = H). For each group,

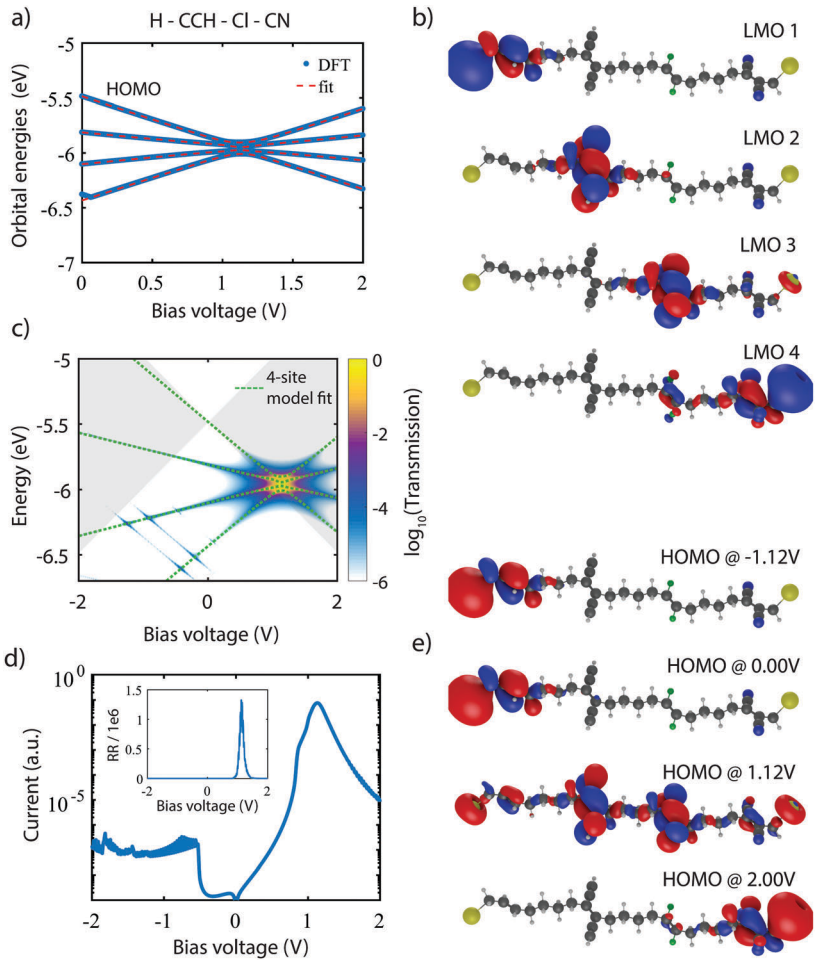

Fig. 3 DFT calculations on the H–CCH–Cl–CN substituted C4-tetraene molecule. (a) Bias dependent DFT calculation (blue), fitted to the four-site model. The obtained fit parameters are $\varepsilon_1 = -5.49$ eV, $\varepsilon_2 = -5.82$ eV, $\varepsilon_3 = -6.10$ eV, $\varepsilon_4 = -6.43$ eV, $\alpha_1 = 0.420$, $\alpha_2 = 0.123$, $\alpha_3 = 0.128$, $\alpha_4 = 0.415$, $\tau_1 = 25.0$ meV, $\tau_2 = 39.0$ meV, $\tau_3 = 28.0$ meV. (b) Localized molecular orbitals, obtained from the molecular orbitals and the fit parameters obtained in (a). (c) Transmission as a function of bias voltage and electron energy, obtained from NEGF calculations using $\Gamma_{L,R} = 100$ meV. The shaded region denotes the bias window. Note in the bottom left corner the presence of additional lines in the transmission. These, however, are located outside the bias window and therefore do not contribute to transport. (d) $\log_{10}(I)$–V characteristic calculated using DFT+NEGF. The inset shows the corresponding rectification ratio; the maximum rectification ratio exceeds 10^6. (e) Effect of the bias voltage on the orbital shape of the HOMO.

the DFT calculation and fitting procedure were performed as described previously. The results are presented in Fig. 2c. The plot shows that the energy of the unsubstituted outer sites ($\varepsilon_{1,4}$) remains approximately constant for all groups. The energies of the inner sites ($\varepsilon_{2,3}$), on the other hand, vary by almost 1.2 eV, between the electropositive methoxy (OCH_3) and the highly electronegative nitro (NO_2). When substituting the outer sites instead of the inner ones, a similar effect is observed (see Fig. 2c). The substituted sites can be varied by 1.4 eV in energy, while the unsubstituted sites remain largely unaffected. The fact to the energy mixing between the sites is small is attributed to the weak coupling between them.

Now that we have shown that the proposed molecule behaves according to the four-site model and that the energy of the sites can be tuned, we proceed to the realisation of a single-molecule diode. As mentioned previously, to achieve this, the sites need to be positioned in a staircase at zero bias, and align at finite bias. Different combinations of side groups can be used to achieve this alignment. Here, as a proof-of-concept, we first focus on the H–CCH–Cl–CN substitution, of which the coordinates and orbital structure can be found in Section V of the ESI.† Further on, we will consider other combinations.

The bias dependent orbital energies of this particular molecule are shown in Fig. 3a. At zero bias, the MOs are split in energy, and hence are the energies of the four sites. At 1.12 V, the MOs align, and diverge again for higher bias voltages. Note that aligning the four sites at the same energy yields four nearly degenerate molecular orbitals, of which the energy splitting depends on the inter-site couplings $\tau_{1,2,3}$. Like in Fig. 3a, the model parameters can be obtained by fitting the MO energies, and are used to validate the four-site model, and to compute the corresponding LMOs. As the fit now requires 11 parameters, a different approach is needed to extract them from the calculations (see Section II of the ESI† or more information). Our starting point is to create two symmetric molecules, one from the left side of the molecule (H–CCH–CCH–H), and one from the right side (CN–Cl–Cl–CN). These symmetric molecules are fitted as described previously. The fitted parameters are then used as initial guesses for a series of unconstrained nonlinear optimization routines. We note that the fitted parameters resulting from these routines do differ from the initial guess. A prediction of the diode properties based on the two symmetric molecules is therefore not straightforward. Importantly, the plot in Fig. 3a shows that the fit reproduces the DFT values well. The LMOs constructed from the fit parameters are depicted in Fig. 3b. Here, again, each LMO is localized on one of the ethylene sites, in accordance with the four-site model.

Using the NEGF formalism, the transmission of the H–CCH–Cl–CN molecule is calculated. Fig. 3c presents a colormap of the logarithm of the transmission as a function of both the bias voltage and the electron energy. Here, the transmission is low everywhere, except at the point at which the four orbitals meet (1.12 V). An important observation is that no other orbital significantly contributes to transport in this bias and energy range, which was one of our design criteria. From the bias-dependent transmission, the current can be calculated. Assuming the HOMO to be on resonance with the Fermi energy at $V = 0$, the IV curve shown in Fig. 3d is obtained. This curve is highly asymmetric, with a large current peak at 1.12 V. At the opposite bias polarity, the current remains orders of magnitude lower. The inset shows the rectification ratio ($|I(V)/I(-V)|$), which reaches as high as 1.3×10^6 at 1.12 V. This large dependence of the current on the bias voltage can also be understood by considering the shape of the MOs upon application of an electric field. Fig. 3e presents the evolution of the wave function of the HOMO with bias voltage. The plot shows that only at a bias voltage of 1.12 V the orbital is fully delocalized across the entire molecule and hence allows for efficient charge transport. For other voltages, the HOMO is highly localized and poorly conducting. A similar trend is observed for the other relevant occupied molecular orbitals, as shown in Section VI of the ESI.†

By varying the chemical substituents, the energies of the four sites can be tuned to meet at a specified bias voltage. In Fig. 3 we used the substituents H–CCH–Cl–CN. In principle, many combinations of substituents are possible (11^4), even tough most of these are not expected to yield a favorable alignment, and hence no large rectification ratio. Due to computational limitations, however, we do not calculate the properties of all these molecules. Instead, we make an educated guess based on the electronegativity/electronpositivity of the groups obtained in Fig. 2. In order to obtain a staircase of the on-site energies, the first site should either be electronpositive or only slightly electronegative (OCH_3, CH_3, H, Br, I, F, CCH, Cl). The second and third site should be slightly to moderately electronegative (H, Br, I, F, CCH, Cl), while the fourth site should be very electronegative (CN, NO_2, CF_3). This choice greatly reduces the number of combinations. For each of the remaining 864 molecules the electronic structure and transmission were calculated as described previously using DFT+NEGF including all orbitals. From the calculated current the rectification ratio, operating voltage and peak current were extracted based on the maximum current in the IV characteristic. Note that no fit parameters are required to obtain these results.

Fig. 4 presents a scatter plot of the obtained rectification ratios *versus* operating voltages, color-coded as a function of the

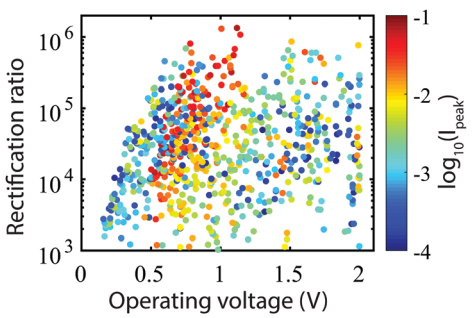

Fig. 4 Rectification ratio *versus* operating voltage. For the 864 molecular combinations, the RR is plotted *versus* the operating voltage, color-coded as a function of respect to the peak current.

peak current. On first sight, a large range of rectification ratios and operating voltages is accessible. However, for many of these combinations, the peak current is low. Interestingly, the high current combinations (red dots) form a cloud which extends from 0.5 V to 1.0 V for ratios varying between 10^4 till 10^6. This cloud is attributed to combinations of side groups of which the sites are well aligned. For more details about the specific side-group combinations, see we refer to Section VII of the ESI.† Within this rectification range, the diode properties can be tuned as desired, albeit with a tendency of having higher rectification at higher operating voltages. This tendency can be attributed to the fact that for higher operating voltages the current in reverse bias mode is suppressed more significantly than for lower operating voltages.

4 Discussion

It is important to keep in mind that in our calculations the HOMO is assumed to be on resonance with the Fermi energy. This alignment is important for reaching the highest rectification ratio; the rectification can experimentally be tuned using a gate electrode, as demonstrate for a two-site molecular rectifier.[15] Fig. 5 presents the dependence of the RR on the alignment of the HOs with the Fermi energy. For a misalignment of 300 meV, the RR is reduced by two orders of magnitude. This can be understood from the transmission plot shown in Fig. 3c. Upon an upward shift of the bias window, the bias window moves away from the region of high transmission, thereby significantly reducing the forward current. The reverse current, however, remains low, and the net result is a decrease in RR.

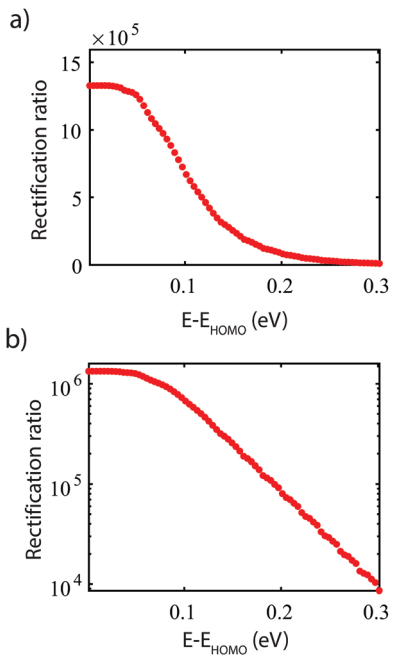

Fig. 5 Influence of the level alignment on the RR. Graph shown on (a) linear scale (b) logarithmic scale.

Another aspect is that the calculations do not take into account dynamical charging effects, *i.e.*, effects due to the addition and removal of electrons as a results of the charge transport through the molecule. To take these effects into account more elaborate calculations involving the GW method would be needed. However, at the moment, such calculations are not feasible for the large molecules considered in this work. Moreover, the influence of the gold electrodes has not explicitly been taken into account, neglecting effects such as the formation of dipoles at the interfaces between the gold and the molecule.[36,37] Therefore, the obtained rectification ratios do not necessarily provide quantitative predictions. We do show, however, that based on the good agreement between DFT and the proposed four-site mode, a molecule consisting of four sites in series may result in a significantly better diode than its two-site counterpart (see Section IV of the ESI† for the two-site molecule). More sophisticated calculations are needed to address these issues.

We further notice that the rectification ratios may be increased even further by adding more sites in series, although this may cause experimental complications, such as reduced solvation and surface mobility, and hence low yields in experimental realization when contacting the molecule. Another restriction is that only a limited amount of side groups is available. The induced shifts are therefore discrete and fine tuning of the alignment of the 4 sites is not straightforward. The range of available energies shift could be greatly increased by using two different side groups per site instead of twice the same.

Moreover, investigating the exact role of the anchoring group may also provide additional insights.[20] In this study, a typical value for the electronic coupling of 100 meV was used, but a wide range in couplings can be achieved by variations in the anchoring groups and/or the binding geometry. In Section I of the ESI,† we show that for a coupling in the range of 10 meV to 300 meV, the rectification ratio varies between 1.2×10^7 and 1.5×10^5. Moreover, we find that applying the coupling in an asymmetrical manner can be used to either enhance or reduce the RR. However, one should keep in mind that changing the anchoring groups also changes the on-site energy, the level alignment, and the inter-site coupling, and that the interplay between these parameters is very delicate.

Finally, we comment on the chemical feasibility of such compounds. To the best of our knowledge, this exact compound or one of the other candidates found in Section VII of the ESI† have not been synthesized. However, the hexane repeat (C–C double bond followed by four saturated CH_2 groups) is found in natural products such as the fulvinols.[38] Shorter repeat units with fewer saturated carbons are highly common in several classes of natural products including terpenes, lipids and vitamins (*e.g.* vitamin K). Most of these products have been synthesized chemically through multiple routes, of which many examples can be found in literature.[39,40] The most important functionalized alkenes have all been synthesized individually, for instance the dichloroalkene,[41] the diacetylene-alkene[42] and the dicyanoalkene.[43] This indicates that in principle the individual groups

are chemically stable and that all parts of the molecule can be synthesized. Investigating whether the exact molecule, or one of the other candidates found in Section VII of the ESI† can be synthesized requires extensive additional synthetic effort, and is beyond the scope of the current study.

5 Conclusions

In conclusion, we provide guide-lines for the design of highly efficient single-molecule rectifiers based on an intuitive four-site model, involving four weakly coupled molecular sites in series. The model gives rise to a single-molecule resonant tunneling diode by aligning the energies of the four sites at a particular bias voltage. Using DFT+NEGF calculations, we explore how chemical substitution of the molecule can be used to control the energy of these sites. With proper choice of the substituents a favorable alignment of the sites can be achieved, leading to highly efficient diodes, with rectification ratios exceeding a million.

Conflicts of interest

There are no conflicts to declare.

Acknowledgements

The authors would like to thank Dr Jos Thijssen for support with the DFT calculations and Dr Michel Calame for careful reading of the manuscript. This research was carried out with financial support from the Dutch Foundation for Fundamental Research on Matter (FOM), the Dutch Organisation for Scientific Research (NWO), the Ministry of Education, Culture and Science (OCW), ERC Grant no. 240299, and by an ERC advanced grant (Mols@Mols).

References

1 M. Souto, L. Yuan, D. C. Morales, L. Jiang, I. Ratera, C. A. Nijhuis and J. Veciana, *J. Am. Chem. Soc.*, 2017, **139**, 4262–4265.
2 L. Qiu, Y. Zhang, T. L. Krijger, X. Qiu, P. van't Hof, J. C. Hummelen and R. C. Chiechi, *Chem. Sci.*, 2017, **8**, 2365–2372.
3 J. A. Smerdon, N. C. Giebink, N. P. Guisinger, P. T. Darancet and J. R. Guest, *Nano Lett.*, 2016, **16**, 2603–2607.
4 N. Nerngchamnong, L. Yuan, D.-C. Qi, J. Li, D. Thompson and C. A. Nijhuis, *Nat. Nanotechnol.*, 2013, **8**, 113–118.
5 L. Yuan, N. Nerngchamnong, L. Cao, H. Hamoudi, E. del Barco, M. Roemer, R. K. Sriramula, D. Thompson and C. A. Nijhuis, *Nat. Commun.*, 2015, **6**, 6324.
6 J. Trasobares, D. Vuillaume, D. Théron and N. Clément, *Nat. Commun.*, 2016, **7**, 12850.
7 X. Chen, M. Roemer, L. Yuan, W. Du, D. Thompson, E. del Barco and C. A. Nijhuis, *Nat. Nanotechnol.*, 2017, **12**, 797–803.
8 M. Elbing, R. Ochs, M. Koentopp, M. Fischer, C. von Hanisch, F. Weigend, F. Evers, H. B. Weber and M. Mayor, *Proc. Natl. Acad. Sci. U. S. A.*, 2005, **102**, 8815–8820.
9 I. Diez-Perez, J. Hihath, Y. Lee, L. Yu, L. Adamska, M. A. Kozhushner, I. I. Oleynik and N. Tao, *Nat. Chem.*, 2009, **1**, 635–641.
10 J. Hihath, C. Bruot, H. Nakamura, Y. Asai, I. Diez-Perez, Y. Lee, L. Yu and N. Tao, *ACS Nano*, 2011, **5**, 8331–8339.
11 E. Lörtscher, B. Gotsmann, Y. Lee, L. Yu, C. Rettner and H. Riel, *ACS Nano*, 2012, **6**, 4931–4939.
12 A. Batra, P. Darancet, Q. Chen, J. S. Meisner, J. R. Widawsky, J. B. Neaton, C. Nuckolls and L. Venkataraman, *Nano Lett.*, 2013, **13**, 6233–6237.
13 T. Kim, Z. F. Liu, C. Lee, J. Neaton and L. Venkataraman, *Proc. Natl. Acad. Sci. U. S. A.*, 2014, **111**, 10928–10932.
14 S. Sherif, G. Rubio-Bollinger, E. Pinilla-Cienfuegos, E. Coronado, J. C. Cuevas and N. Agraït, *Nanotechnology*, 2015, **26**, 291001.
15 M. L. Perrin, E. Galán, R. Eelkema, J. M. Thijssen, F. Grozema and H. S. van der Zant, *Nanoscale*, 2016, **8**, 8919–8923.
16 C. Guo, K. Wang, E. Zerah-Harush, J. Hamill, B. Wang, Y. Dubi and B. Xu, *Nat. Chem.*, 2016, **8**, 484–490.
17 A. Aviram and M. A. Ratner, *Chem. Phys. Lett.*, 1974, **29**, 277–283.
18 M. L. Perrin, R. Frisenda, M. Koole, J. S. Seldenthuis, J. A. Celis Gil, H. Valkenier, J. C. Hummelen, N. Renaud, F. C. Grozema, J. M. Thijssen, D. Dulić and H. S. J. van der Zant, *Nat. Nanotechnol.*, 2014, **9**, 830–834.
19 K. Stokbro, J. Taylor and M. Brandbyge, *J. Am. Chem. Soc.*, 2003, **125**, 3674–3675.
20 M. L. Perrin, E. Galan, R. Eelkema, F. C. Grozema, J. M. Thijssen and H. S. J. van der Zant, *J. Phys. Chem. C*, 2015, **119**, 5697–5702.
21 C. Van Dyck and M. A. Ratner, *Nano Lett.*, 2015, **15**, 1577–1584.
22 M. Kilgour and D. Segal, *J. Phys. Chem. C*, 2017, **119**, 25291–25297.
23 Y. Meir and N. S. Wingreen, *Phys. Rev. Lett.*, 1992, **68**, 2512–2515.
24 A.-P. Jauho, N. S. Wingreen and Y. Meir, *Phys. Rev. B: Condens. Matter Mater. Phys.*, 1994, **50**, 5528–5544.
25 H. Haug and A.-P. Jauho, *Quantum Kinetics in Transport and Optics of Semiconductors*, Springer, Berlin, Heidelberg, 1997.
26 Z.-L. Cheng, R. Skouta, H. Vazquez, J. R. Widawsky, S. Schneebeli, W. Chen, M. S. Hybertsen, R. Breslow and L. Venkataraman, *Nat. Nanotechnol.*, 2011, **6**, 353–357.
27 J. R. Widawsky, W. Chen, H. Vázquez, T. Kim, R. Breslow, M. S. Hybertsen and L. Venkataraman, *Nano Lett.*, 2013, **8**, 2889–2894.
28 A. Etcheverry-Berríos, I. Olavarría, M. L. Perrin, R. Díaz-Torres, D. Jullian, I. Ponce, J. H. Zagal, J. Pavez, S. O. Vásquez, H. S. J. van der Zant, D. Dulić, N. Aliaga-Alcalde and M. Soler, *Chem. – Eur. J.*, 2016, **22**, 12808–12818.
29 I. Díez-Pérez, Z. Li, S. Guo, C. Madden, H. Huang, Y. Che, X. Yang, L. Zang and N. Tao, *ACS Nano*, 2012, **6**, 7044–7052.
30 M. Baghernejad, D. Z. Manrique, C. Li, T. Pope, U. Zhumaev, I. Pobelov, P. Moreno-García, V. Kaliginedi, C. Huang, W. Hong, C. Lambert and T. Wandlowski, *Chem. Commun.*, 2014, **50**, 15975–15978.

31 B. Capozzi, Q. Chen, P. Darancet, M. Kotiuga, M. Buzzeo, J. B. Neaton, C. Nuckolls and L. Venkataraman, *Nano Lett.*, 2014, **14**, 1400–1404.
32 M. L. Perrin, E. Burzurí and H. S. J. van der Zant, *Chem. Soc. Rev.*, 2015, **44**, 902–919.
33 G. te Velde, F. M. Bickelhaupt, S. J. A. van Gisbergen, C. Fonseca Guerra, E. J. Baerends, J. G. Snijders and T. Ziegler, *J. Comput. Chem.*, 2001, **22**, 931–967.
34 C. Fonseca Guerra, J. G. Snijders, G. te Velde and E. J. Baerends, *Theor. Chem. Acc.*, 1998, **99**, 391–403.
35 C. J. O. Verzijl, J. S. Seldenthuis and J. M. Thijssen, *J. Chem. Phys.*, 2013, **138**, 094102.
36 G. Heimel, E. Zojer, L. Romaner, J.-L. Brédas and F. Stellacci, *Nano Lett.*, 2009, **9**, 2559–2564.
37 C. Van Dyck and M. A. Ratner, *J. Phys. Chem. C*, 2017, **121**, 3013–3024.
38 M. L. Ciavatta, G. Nuzzo, K. Takada, V. Mathieu, R. Kiss, G. Villani and M. Gavagnin, *J. Nat. Prod.*, 2014, **77**, 1678–1684.
39 A. M. Daines, R. J. Payne, M. E. Humphries and A. D. Abell, *Curr. Org. Chem.*, 2003, **7**, 1–15.
40 T. J. Maimone and P. S. Baran, *Nat. Chem. Biol.*, 2007, **3**, 396–407.
41 T. Schlama, K. Gabriel, V. Gouverneur and C. Mioskowski, *Angew. Chem., Int. Ed.*, 1997, **36**, 2342–2344.
42 J.-F. Nierengarten, D. Guillon, B. Heinrich and J.-F. Nicoud, *Chem. Commun.*, 1997, 1233–1234.
43 S. Arai, T. Sato and A. Nishida, *Adv. Synth. Catal.*, 2009, **351**, 897–1904.

